ACTA ET COMMENTATIONES UNIVERSITATIS TARTUENSIS DE MATHEMATICA
Volume 23, Number 2, December 2019
Available online at http://acutm.math.ut.ee

Theoretical description of large deformations in criss-cross composites (with application to Tensylon®)

Pavel S. Mostovykh

Abstract. A theoretical model of an anisotropic material, Tensylon®, under large strains is proposed. This model is capable to describe the material's response in in-plane tension at different angles to the fibrils. At 0° and at 90°, i.e., along the fibrils in either "criss" or "cross" plies, it quantitatively predicts the experimentally observed elastic behaviour until failure. At 45° to the fibrils, it quantitatively describes the experimental data in the elastic and plastic domains. The description remains accurate up to strains of 35%, that corresponds to $30 \div 40\%$ of deformation gradient components. The infinitesimal strains model would give at least 25% of error under such circumstances.

1. Introduction

Tensylon® HSBD 30A is a bidirectional laminate, representative of the ultra high molecular weight polyethylene (UHMWPE) material produced by the melt spinning manufacturing technology [5, 6], followed by a combination of solid-state extrusion (SSE) and drawing. The DuPont$^{\text{TM}}$ company fabricates it in the form of 1.600 ± 0.013 m wide, ≥ 300 m long, ~ 120 μm thick tape with an areal density of 111 g/m^2 $\pm 6\%$ [4] consisting of two plies. Each ply is produced by stretching in a particular direction (direction of the fibrils), and therefore it is approximately transversely isotropic with the characteristic direction of stretching. The tape has a criss-cross structure, i.e., it can be described by the [0°/90°] structural formula.

In structural applications, UHMWPE are primarily known as a material for ropes. However, it is a perspective material for applications as shells also, particularly for high pressure vessels and pipes. As an anisotropic material

Received November 1, 2018.
2010 *Mathematics Subject Classification.* 74B20; 74C15; 74Q15.
Key words and phrases. Elastoplasticity; large strains; criss-cross composites; UHMWPE; Tensylon®; true/Piola–Kirchhoff stress tensors.
https://doi.org/10.12697/ACUTM.2019.23.23

with complex internal structure, its properties are significantly different in different directions; the characteristic values are the following:

- the ultimate stress along the fibrils (i.e., in the 0° and 90° directions) in tension is $\sim$ 500 MPa, whereas in compresssion $\sim$ 10 MPa (the value is uncertain since structural instability and kinking occurs under compression); in the through-thickness direction the strength in tension is low (because of inter-ply delamination), whereas in compression it reaches $\sim$ 700 MPa, and in shear yield begins at $5 \div 30$ MPa (this value is also characteristic for in-plane tension non parallel to the fibrils);
- the achievable strains are $\sim 2\%$ in tension along the fibrils, $\sim 15\%$ in through-thickness compression, $\sim 20°$ in in-plane shear;
- with a density of 0.94–0.97 g/cm^3, this material floats in water;
- with the glass transition temperature of 130°–155° C depending on the molecular weight, the material's applicability is limited to room and cold-temperature applications;
- the material's thickness can go from the original tape thickness of 120 μm up to 22 mm pressed plates of various geometries;
- the material is chemically and environmentally stable under various loads.

In [2], a visco-elasto-plastic description of Tensylon® is proposed. It satisfactorily describes the material's properties along the fibrils' direction in simple loadings at constant strain rate, loadings with stress relaxation and with inverse stress relaxation, as well as cyclic loadings, with overall duration between 30 s and 3 h. However, since the material of interest is anisotropic, tensile properties along a given direction do not fully characterize the material' mechanical behaviour.

Mechanical properties in a variety of directions for Tensylon® were considered in [1]. The material's response to in-plane shear was experimentally shown to be elasto-plastic. The experiments in [1] were performed on the Lloyd LR5KPlus universal materials testing machine in-plane at an angle of 45° to the fibrils direction in both 0° and 90° plies. Since the longitudinal strain reached the values as high as 40%, the mechanics of small (infinitesimal) strains is not applicable to describe the full curve. In view of this, [1] considered only the elastic and the early plastic part of the experimental curves, and reached a conclusion that the strain hardening follows a linear law. The fact that the elastic modulus increases with the plastic strain was evidenced by plotting the corresponding dependence, but no theoretical explanation to this fact was proposed.

In the present paper, the elasto-plastic model of in-plane shear is revisited. By applying a consistent large deformation theory [7, 8, 9], the material's shear stress-shear strain curve is calculated from the experimental data. It

is shown that, unlike the infinitesimal strain case, the purely elastic release from a deformed state does not coincide with the initial loading from the material virgin state. The repeatability of the experimental results is also analysed.

2. Construction of the rheological model

2.1. Governing relations. As long as non-infinitesimal strains are concerned, the strain tensor and the stress tensor components along a set of directions fixed within the body and fixed within the surrounding become different quantities. In what follows, we use the approach and the notations of the books [7, 8], i.e., we consider that the deformation occurs with respect to the fixed orthonormal Cartesian system of coordinates, and the material's system of coordinates in the undeformed state is also a fixed orthonormal Cartesian system of coordinates (although rotated with respect to the former). Where necessary, we compare these formulae with the results of [9] simplified for the aforementioned case.

Within the material, we will use the system of axes 1 for the fibrils direction, 2 for the in-plane direction initially perpendicular to it, and 3 for the out-of-plane direction. In the "criss" and "cross" plies, the 1 and 2 directions interchange. Where significant, the superscipt "+" refers solely to the "criss" and the superscipt "−" refers solely to the "cross" plies; for example, the previous statement can be expressed as $1^+ \parallel 2^-$, $1^- \parallel 2^+$. Within the surrounding, we will use x for the direction of loading (45° to the fibrils in all plies), y for its in-plane perpendicular and z for the out-of-plane direction. When the deformation occurs, the material-based coordinates system does not remain orthogonal, as can be seen in Figure 1. The symmetry considerations allow to express all the angles through a single value θ: $\angle(1, x) = \angle(2, x) = \theta$, $\angle(1, y) = \angle(2, y) = \pi/2 - \theta$, $\angle(3, z) = 0$, where $\theta \le \pi/4$, and the remaining angles are $\pi/2$.

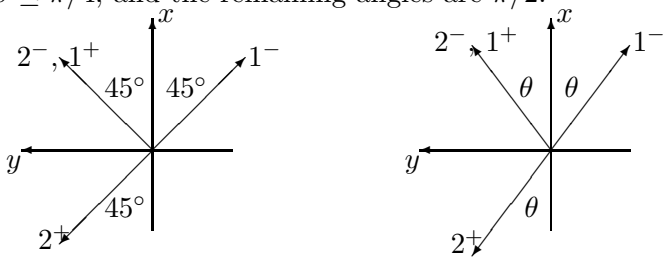

FIGURE 1. The coordinates system in the material's undeformed state (left) and its deformed state (right).

First, we give a complete description of the deformation process in terms of displacements and strains, where it is convenient to start in the surrounding-based (x, y, z) frame, and then transfer to the material-based (1, 2, 3) frame. Then, we propose the material's rheological model in terms of the specific

energy in the elasto-plastic loading, and independently in terms of the purely elastic energy that is required to assess the material's properties in elastic release processes. Finally, we give the process description in terms of stress. Here, the order opposite to that in strains is more appropriate: we begin with the second Piola–Kirchhoff stress tensor, that is defined in the material-based frame, and therefore in different frames for the "criss" and the "cross" plies, then obtain the true (Cauchy) and the engineering (Lagrangian) stress tensors for each of the plies, and proceed for the average stress tensor of the material.

2.1.1. *Strains.* Since the criss-cross laminate as a whole is symmetric with respect to the x, y, and z axes, no shear occurs in this frame of reference, i.e.,

$$u = E_x x, \qquad v = E_y y, \qquad w = E_z z,$$

where u, v, w are the point (x, y, z) displacements along the axes x, y, z, respectively, and E_x, E_y, E_z — engineering strains (stretches). Neglecting the edge effects, the stretches are constant throughout the whole active area of the sample. In this case, the strain tensor is readily obtained:

$$\varepsilon_{ij} = \operatorname{diag}\{E_x(1 + E_x/2),\, E_y(1 + E_y/2),\, E_z(1 + E_z/2)\},$$

and the strain tensors in the ply coordinates are given by 45° rotation clockwise for the minus ply and counter-clockwise for the plus ply:

$$\varepsilon^{\pm}_{ij} = \begin{pmatrix} ((1+E_x)^2+(1+E_y)^2-2)/4 & \mp(E_x-E_y)(1+(E_x+E_y)/2) & 0 \\ \mp(E_x-E_y)(1+(E_x+E_y)/2) & ((1+E_x)^2+(1+E_y)^2-2)/4 & 0 \\ 0 & 0 & E_z(1+E_z/2) \end{pmatrix}. \quad (1)$$

(In the [9] notation, the shear elements are twice smaller.) In what follows, we will use the fibril strain

$$E_{\mathrm{s}} = \sqrt{1 + 2((1 + E_x)^2 + (1 + E_y)^2 - 2)/4} - 1$$

and the angle θ rather than E_x and E_y. Since $\angle(1^+, 2^+) = \pi - 2\theta$ and $\angle(1^-, 2^-) = 2\theta$, its cosine is

$$\mp\cos 2\theta = \varepsilon^{\pm}_{xy}/(1+E_{\mathrm{s}})^2 = \mp(E_x-E_y)\,(1 + (E_x+E_y)/2)/\big((1+E_x)^2+(1+E_y)^2\big)\cdot 2,$$

and E_x, E_y can be expressed as

$$E_x = (1 + E_{\mathrm{s}})\sqrt{2}\cos\theta - 1, \qquad E_y = (1 + E_{\mathrm{s}})\sqrt{2}\sin\theta - 1.$$

The deformation gradient tensors for both plies will also be required. In this particular case, they are symmetric (i.e., neither of the plies exhibits a curl), and take the form

$$e^{\pm}_{ij} = \begin{pmatrix} (1+E_{\mathrm{s}})(\cos\theta+\sin\theta)/\sqrt{2}-1 & \mp(1+E_{\mathrm{s}})\sqrt{2}(\cos\theta-\sin\theta) & 0 \\ \mp(1+E_{\mathrm{s}})\sqrt{2}(\cos\theta-\sin\theta) & (1+E_{\mathrm{s}})(\cos\theta+\sin\theta)/\sqrt{2}-1 & 0 \\ 0 & 0 & E_z \end{pmatrix}. \quad (2)$$

2.1.2. *Rheology.* The expression for the specific energy used hereinafter is an extension of the proposed in [1]. Similarly, the specific energy is considered as a sum of the fibril tensile energy, shear energy in the planes containing fibrils, and the energy in the perpendicular plane that is considered isotropic (i.e., the material of each ply is assumed to be transversely isotropic):

$$\Phi^{\pm} = E_{\mathrm{f}} {\varepsilon_{xx}^{\pm}}^2/2 + \Phi_{\mathrm{s}}\left(\Upsilon_{\varepsilon}\right) + \frac{E_{\mathrm{m}}}{2(1-\nu^2)}\left(\varepsilon_{yy}^{\pm} + \varepsilon_{zz}^{\pm}\right)^2 - \frac{E_{\mathrm{m}}}{1+\nu}\left(\varepsilon_{yy}^{\pm}\varepsilon_{zz}^{\pm} - {\varepsilon_{yz}^{\pm}}^2/4\right), \tag{3}$$

where

$$\Upsilon_{\varepsilon} = \sqrt{{\varepsilon_{xy}^{\pm}}^2 + {\varepsilon_{xz}^{\pm}}^2},$$

E_{f} is the Young modulus in the fibre direction 1, E_m is the Young modulus in the transverse directions 2 and 3, ν is the Poisson ratio relating stress in direction 2 with strain in direction 3 and vice versa, $\Phi_{\mathrm{s}}(\varepsilon)$ is a non-linear function of its argument that specifies the energy required to impose pure shear on the material of interest.

The fibril energy is purely elastic, and this fact is experimentally validated [1]. The expression for the energy in the perpendicular plane is not directly validated; however, in the particular case studied, the strains ε_{yy}, ε_{zz} are of the same order as ε_{xx}, and since $E_{\mathrm{m}} \ll E_{\mathrm{f}}$, the third and the fourth terms are small compared to the first. Non-linear and/or irreversible effects in the plane perpendicular to the fibrils are neither significant in the considered type of loading nor measurable within the amount of testing fulfilled. Nevertheless, we provide here the full expression for the specific energy, with the coefficients expressed through the "matrix" Young modulus and Poisson ratio specifically for the transversally isotropic type of symmetry. The second term is the subject of the present study.

Release from the deformed state does not follow the same path as the previous loading, and therefore another expression for the specific energy should then be used. The expression for the release specific energy $\Phi_{\mathrm{r}}^{\pm}$ includes all the terms present in (3), with the shear energy calculated for the maximum strain $\Phi_{\mathrm{s}}\left(\max \Upsilon_{\varepsilon}\right)$, and in addition the following terms:

$$\Phi_{\mathrm{r}}^{\pm} = G_{\mathrm{s}}\left(\max \Upsilon_{\varepsilon} - \Upsilon_{\varepsilon}\right)^2/2 - \Phi_{\mathrm{s}}'\left(\max \Upsilon_{\varepsilon}\right)\left(\max \Upsilon_{\varepsilon} - \Upsilon_{\varepsilon}\right) + \ldots,$$

where G_{s} is the elastic shear modulus. So defined, the specific energy remains continuous, as well as its derivatives, i.e., stresses. In other words, the release is assumed to be purely elastic, the shear modulus to be independent of the preliminary plastic strain, and the formulation is provided for the simple loads in the $(\varepsilon_{xy}^{\pm}, \varepsilon_{xz}^{\pm})$ space only.

2.1.3. *Stresses.* The second Piola–Kirchhoff stress tensor during primary loading is readily obtained by differentiation of the specific energy (3) with respect to strains. In the general case, it is given by:

$$\sigma_{ij}^{*\,\pm} = \begin{pmatrix} E_\mathrm{f}\varepsilon_{xx}^{\pm} & \frac{\Phi_\mathrm{s}'(\Upsilon_\varepsilon)}{\Upsilon_\varepsilon}\varepsilon_{xy}^{\pm} & \frac{\Phi_\mathrm{s}'(\Upsilon_\varepsilon)}{\Upsilon_\varepsilon}\varepsilon_{xz}^{\pm} \\ \frac{\Phi_\mathrm{s}'(\Upsilon_\varepsilon)}{\Upsilon_\varepsilon}\varepsilon_{xy}^{\pm} & E_\mathrm{m}\big(\varepsilon_{yy}^{\pm}+\nu\varepsilon_{zz}^{\pm}\big)/(1-\nu^2) & E_\mathrm{m}\varepsilon_{yz}^{\pm}/(2(1+\nu)) \\ \frac{\Phi_\mathrm{s}'(\Upsilon_\varepsilon)}{\Upsilon_\varepsilon}\varepsilon_{xz}^{\pm} & E_\mathrm{m}\varepsilon_{yz}^{\pm}/(2(1+\nu)) & E_\mathrm{m}\big(\varepsilon_{zz}^{\pm}+\nu\varepsilon_{yy}^{\pm}\big)/(1-\nu^2) \end{pmatrix}. \tag{4}$$

For our case of the strain tensor given by (1), the stress tensor (4) reduces to

$$\sigma_{ij}^{*\,\pm} = \begin{pmatrix} E_\mathrm{f}E_\mathrm{s}(1+E_\mathrm{s}/2) & \Phi_\mathrm{s}'\big(\mp(1+E_\mathrm{s})^2\cos 2\theta\big) & 0 \\ \Phi_\mathrm{s}'\big(\mp(1+E_\mathrm{s})^2\cos 2\theta\big) & E_\mathrm{m}\mathcal{E}_{sz}/(1-\nu^2) & 0 \\ 0 & 0 & E_\mathrm{m}\mathcal{E}_{zs}/(1-\nu^2) \end{pmatrix}$$

where

$$\mathcal{E}_{ut} = E_\mathrm{u}(1+E_\mathrm{u}/2) + \nu E_t(1+E_t/2).$$

Since the specific energy Φ_s is an odd function of its argument, its derivative is an even function, and the $\pm$ sign can be extracted outside the function. For the plane stress conditions we assume, $E_z(1+E_z/2)+\nu E_\mathrm{s}(1+E_\mathrm{s}/2)=0$, that gives us the expression for the out-of-plane strain $E_z \approx -\nu E_\mathrm{s}$.

The true stress (in the Cartesian coordinates aligned with the undeformed orientations of (1, 2, 3), i.e., at 45° to the (x, y, z) frame) can, for example, be obtained by multiplication of three matrices:

$$\begin{aligned} \sigma_{ij} = &\begin{pmatrix} (1+E_\mathrm{s})(\cos\theta+\sin\theta)/\sqrt{2} & \mp(1+E_\mathrm{s})(\cos\theta-\sin\theta)/\sqrt{2} & 0 \\ \mp(1+E_\mathrm{s})(\cos\theta-\sin\theta)/\sqrt{2} & (1+E_\mathrm{s})(\cos\theta+\sin\theta)/\sqrt{2} & 0 \\ 0 & 0 & 1+E_z \end{pmatrix} \\ &\times \begin{pmatrix} E_\mathrm{f}E_\mathrm{s}(1+E_\mathrm{s}/2) & \mp\Phi_\mathrm{s}'\left((1+E_\mathrm{s})^2\cos 2\theta\right) & 0 \\ \mp\Phi_\mathrm{s}'\left((1+E_\mathrm{s})^2\cos 2\theta\right) & E_\mathrm{m}E_\mathrm{s}(1+E_\mathrm{s}/2) & 0 \\ 0 & 0 & 0 \end{pmatrix} \\ &\times \begin{pmatrix} (1+E_\mathrm{s})(\cos\theta+\sin\theta)/\sqrt{2} & \mp(1+E_\mathrm{s})(\cos\theta-\sin\theta)/\sqrt{2} & 0 \\ \mp(1+E_\mathrm{s})(\cos\theta-\sin\theta)/\sqrt{2} & (1+E_\mathrm{s})(\cos\theta+\sin\theta)/\sqrt{2} & 0 \\ 0 & 0 & 1+E_z \end{pmatrix} \frac{1}{D} \end{aligned} \tag{5}$$

where D is the determinant of the last matrix. After multiplication, these tensors are rotated 45° to the original (x, y, z) frame. It turns out that $\sigma_{xx}^{+} = \sigma_{xx}^{-}$, i.e., the tensile stresses along the loading are the same in the "criss" and "cross" plies, and $\sigma_{yy}^{+} = \sigma_{yy}^{-}$. These latter stresses should vanish (since the sample side walls are free of stress), and therefore a relation between E_s and θ is obtained. On the contrary, $\sigma_{xy}^{+} = -\sigma_{xy}^{-}$, i.e., the shear stresses that should be applied on the loading, as well as on the side areas of the sample, are, on average, zero. However, they are non-zero for each ply, that means that a special type of "edge effects" occur in the material under 45° tension. While the "edge effects" in the clamped parts of the sample are insignificant, the "edge effects" on the sides of the sample are likely to influence the sample

failure process, and can also cause the engineering stress-strain diagrams dependence on the width of the sample. However, this dependence has not been studied experimentally.

On the last step, $\sigma_{xx}^{\pm}$ should be recalculated for the engineering stress, in order to provide comparison with the experimental data (experimental strain is given by E_x, and both the stress and strain are expressed through θ, so that the stress-strain curve is obtained in a parametric form).

Alternatively, the stresses $\vec{\sigma}_{n_1}$, $\vec{\sigma}_{n_2}$, $\vec{\sigma}_{n_3}$, that appear in the non-linear theory, can be evaluated. They are defined as stresses acting on the surfaces that used to be perpendicular to the coordinate axes 1, 2, 3 before the deformation; therefore, $\angle(n_1,\, x) = \angle(n_2,\, x) = \pi/2 - \theta$, $\angle(n_1,\, y) = \angle(n_2,\, y) = \theta$, $\angle(n_3,\, z) = 0$, the remaining angles are $\pi/2$. These respective vectors $\vec{\sigma}_{n_1}$, $\vec{\sigma}_{n_2}$, $\vec{\sigma}_{n_3}$ are projected along the three non-orthogonal directions 1, 2, 3 to form a nine-element stress matrix, that is non-symmetric in general and that we would denote σ_{11}–σ_{33}. It has been shown [7, 8], that the aforementioned matrix σ_{ij}^{*} can, in terms of

$$\mathcal{Q}_{i\varepsilon} = \sqrt{(1+2\varepsilon_{ii})(1+2\varepsilon_{33}) - \varepsilon_{i3}^{2}}, \;\; i = 1, 2,$$

be expressed as

$$\begin{pmatrix} \mathcal{Q}_{2\varepsilon}\frac{\sigma_{11}}{\sqrt{1+2\varepsilon_{11}}} & \mathcal{Q}_{2\varepsilon}\frac{\sigma_{12}}{\sqrt{1+2\varepsilon_{22}}} \\ \mathcal{Q}_{1\varepsilon}\frac{\sigma_{21}}{\sqrt{1+2\varepsilon_{11}}} & \mathcal{Q}_{1\varepsilon}\frac{\sigma_{22}}{\sqrt{1+2\varepsilon_{22}}} \end{pmatrix}$$

with the remaining elements being zeros. In our particular case, the σ_{11}–σ_{33} differs from σ_{ij}^{*} by a factor of $(1 + E_z)$.

The conditions on the loading planes and on the lateral planes, averaged between the "criss" and "cross" plies, read

$$\begin{aligned} &\mathcal{Q}_{2\varepsilon}(\vec{\sigma}_{n_1}^{+} + \vec{\sigma}_{n_1}^{-})/\sqrt{2} + \mathcal{Q}_{1\varepsilon}(\vec{\sigma}_{n_2}^{-} - \vec{\sigma}_{n_2}^{+})/\sqrt{2} = 2t_{45}\vec{e}_x, \\ &\mathcal{Q}_{2\varepsilon}(\vec{\sigma}_{n_1}^{+} - \vec{\sigma}_{n_1}^{-})/\sqrt{2} + \mathcal{Q}_{1\varepsilon}(\vec{\sigma}_{n_2}^{+} + \vec{\sigma}_{n_2}^{-})/\sqrt{2} = 0, \end{aligned} \tag{6}$$

where t_{45} is the engineering stress in the direction of loading, related to the true stress σ_{45} according to the formula $t_{45} = (S_n^{*}/S_n)\,\sigma_{45}$, where S_n^{*} and S_n are the deformed and undeformed area, respectively. The relations (6), projected on the x and y directions, respectively, give

$$\begin{aligned} &\mathcal{Q}_{2\varepsilon}\big(2\sigma_{11} + (\sigma_{12}^{-} - \sigma_{12}^{+})\big)\cos\theta/\sqrt{2} + \mathcal{Q}_{1\varepsilon}\big((\sigma_{21}^{-} - \sigma_{21}^{+}) + 2\sigma_{22}\big)\cos\theta/\sqrt{2} = 2t_{45}, \\ &\mathcal{Q}_{2\varepsilon}\big(2\sigma_{11} + (\sigma_{12}^{+} - \sigma_{12}^{-})\big)\sin\theta/\sqrt{2} + \mathcal{Q}_{1\varepsilon}\big((\sigma_{21}^{+} - \sigma_{21}^{-}) + 2\sigma_{22}\big)\sin\theta/\sqrt{2} = 0, \end{aligned}$$

whereas the other two projections, taking into account the ply symmetry/anti-symmetry conditions, result in identities $0 = 0$. Subtracting equations, we arrive at

$$\mathcal{Q}_{2\varepsilon}(\sigma_{12}^{-} - \sigma_{12}^{+})\cos\theta/\sqrt{2} + \mathcal{Q}_{1\varepsilon}(\sigma_{21}^{-} - \sigma_{21}^{+})\cos\theta/\sqrt{2} = t_{45}, \tag{7}$$

that gives us a remarkable result that the measured 45° tensile response is fully driven by the shear stress in the ply characteristic directions. Simplifying, we get

$$|\sigma_{12}| = t_{45}/[2\sqrt{2}(1+E_{\mathrm{s}})(1+E_z)\cos\theta]$$

and $t_{45}/2$ in the infinitesimal strains domain ($E_{\mathrm{s}} \ll 1$, $E_z \ll 1$, $\pi/4-\theta \ll 1$). This is a well-known fact that the shear stress at 45° to the direction of uniaxial loading is twice as big as the applied stress; as can be seen, it is valid only for infinitesimal strains.

During the stress release, the second Piola–Kirchhoff stress tensor ${\sigma^*_{ij}}^{\pm}$ becomes

$$\begin{pmatrix} E_{\mathrm{f}}E_{\mathrm{s}}(1+E_{\mathrm{s}}/2) & \Phi'_{\mathrm{s}}\big(\gamma^{\pm}_{\max}\big)-G_{\mathrm{s}}\big(\gamma^{\pm}_{\max}\pm(1+E_{\mathrm{s}})^2\cos 2\theta\big) & 0 \\ \Phi'_{\mathrm{s}}\big(\gamma^{\pm}_{\max}\big)-G_{\mathrm{s}}\big(\gamma^{\pm}_{\max}\pm(1+E_{\mathrm{s}})^2\cos 2\theta\big) & E_{\mathrm{m}}E_{\mathrm{s}}(1+E_{\mathrm{s}}/2) & 0 \\ 0 & 0 & 0 \end{pmatrix},$$

where $\gamma^{\pm}_{\max}$ is the extremum value of $\varepsilon^{\pm}_{xy}$, i.e., $\gamma^{+}_{\max} < 0$ and $\gamma^{-}_{\max} > 0$. It can be verified that the remaining derivations, including (7), remain valid during the release phase.

2.2. Application to Tensylon®. The experiments at an angle of 45° to the fibrils direction in both "criss" and "cross" plies were performed on the Lloyd LR5KPlus universal materials testing machine, and are described in detail in [1]. They included loading at a given strain rate $2.1 \cdot 10^{-2}$ 1/s, and ocassionally done releases and re-loads at the same strain rate. Using the formulae (7) and (1), these data can be represented in terms of the shear stress $\tau \equiv \big|{\sigma^*_{12}}^{\pm}\big|$ and the shear angle $\gamma \equiv \big|\varepsilon^{\pm}_{12}\big|$. The resulting curves for three different samples are presented in Figure 2.

The data of Figure 2 suggests that the material's behaviour is relatively repeatable up to failure, that is quite unusual for new polymeric materials and large angles that reach 0.8–0.9 rad. The elastic part of the curve is described by the shear modulus ($\tau = G_{\mathrm{s}}\gamma$, $G_{\mathrm{s}} = 750$ MPa), and the plastic part was fitted with a linear law of strengthening: $\tau = p_0 + p_1\gamma$, where $p_0 = 16.5$ MPa, $p_1 = 24.5$ MPa. The elasto-plastic transition occurs at $\tau_{\mathrm{p}} = 17$ MPa, and the engineering yield limit is negligibly larger; the engineering stress in the 45° tension is then 35 MPa, i.e., slightly more than twice higher. The function $\Phi_{\mathrm{s}}(\varepsilon)$ in (3) is, therefore, given by

$$\Phi_{\mathrm{s}}(\varepsilon) = \begin{cases} G_{\mathrm{s}}\varepsilon^2/2, & \varepsilon \le \tau_{\mathrm{p}}/G_{\mathrm{s}}, \\ (p_0+p_1\varepsilon)^2/(2p_1)+\tau_{\mathrm{p}}^2/(2G_{\mathrm{s}})-(p_0+p_1\tau_{\mathrm{p}}/G_{\mathrm{s}})^2/(2p_1), & \varepsilon \ge \tau_{\mathrm{p}}/G_{\mathrm{s}}. \end{cases} \tag{8}$$

The presented model reasonably well describes the overall behaviour of Tensylon® (Figures 3 and 4). In particular, the present analysis shows that strengthening occurs both due to physical non-linearity (physical strengthening, described by the value p_1) and to geometrical non-linearity (rotation of the fibres towards the direction of loading that results in the increase of

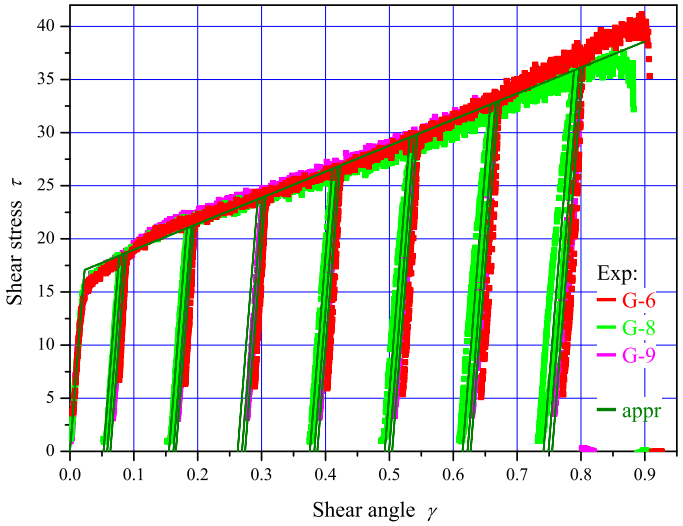

FIGURE 2. Experimental data recalculated for the shear stress-shear strain, and its fit in the elastic and plastic domains.

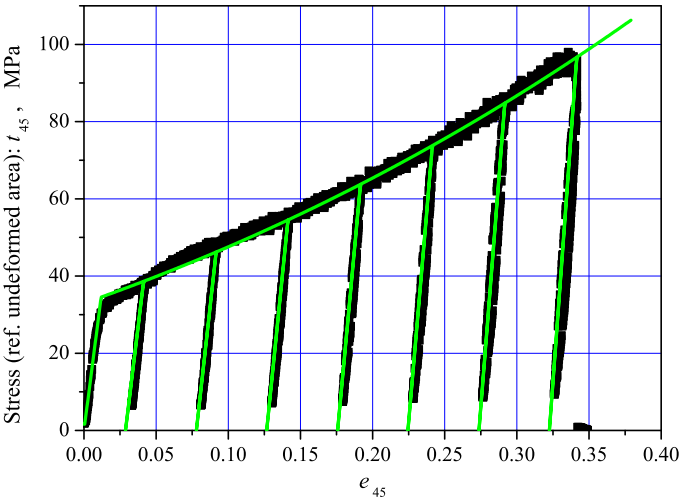

FIGURE 3. Comparison of the experimental and the predicted stress-strain curve in 45° tension. Stress was calculated with reference to the undeformed body area (engineering/first Piola–Kirchhoff stress), strain was calculated as a non-dimensional machine cross-head displacement (a component of the deformation gradient tensor). Sample G–9.

stress). Both the experimental and the predicted strengthening curves in Figures 3 and 4 are non-linear, with the tangential modulus increasing with strain— this effect is shown to be of geometrical nature.

In order to compare more accurately, the variation of the material's modulus with plastic strain was theoretically calculated, and compared with the experimental results (Figure 5). The experimental points represent the average modulus that was obtained by simultaneous fit of the unloading and the subsequent loading points (notwithstanding some minor hysteresis between unloading and subsequent loading, that is, most like by a sign of the viscoelastic effects present in the material). It can be seen that the sample-to-sample variation in this particular characteristic was significant, and the theoretical prediction lies within the scatter. The proposed theory suggests that the modulus increases with plastic strain at all values, whereas some experimental data does not: the modulus increases at the beginning, but at high strains it stabilizes, or even decreases. It is likely that the material failure does not occur all-at-once, but constitutes a long-lasting phenomenon.

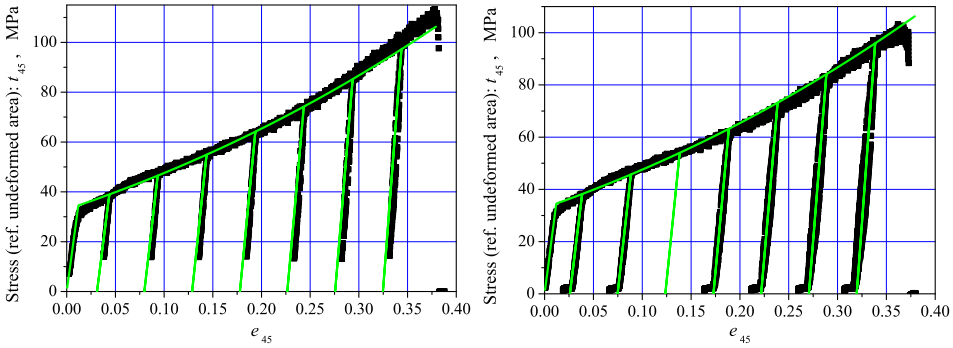

FIGURE 4. Comparison of the experimental and the predicted stress-strain curve in 45° tension. Stress was calculated with reference to the undeformed body area (engineering/first Piola–Kirchhoff stress), strain was calculated as a non-dimensional machine cross-head displacement (a component of the deformation gradient tensor). Sample G–6 (left), G–8 (right).

The proposed theory suggests that the sum of the sample strains, $\varepsilon_{xx}+\varepsilon_{yy}$, remains very small (not exceeding 0.3%), so that $E_x + E_y < 0$. The lateral deformation was not measured during the test, but post-mortem (after the sample failure) its linear dimensions were estimated. It was not possible to measure accurately (the width absolute accuracy of 0.5 mm means relative accuracy of 7% at best), but the approximate values of $E_x \approx 30\%$, $E_y \approx -40$, and $\varepsilon_{xx} + \varepsilon_{yy} \approx 2 \div 4\%$ were revealed. For a sample loaded up to 83 MPa (engineering stress) and released without failure, $|\varepsilon_{xx} + \varepsilon_{yy}|$ below 0.5% was measured. The front face area decreases to $\approx 80\%$ of its initial value. Therefore, the theory predictions are confirmed.

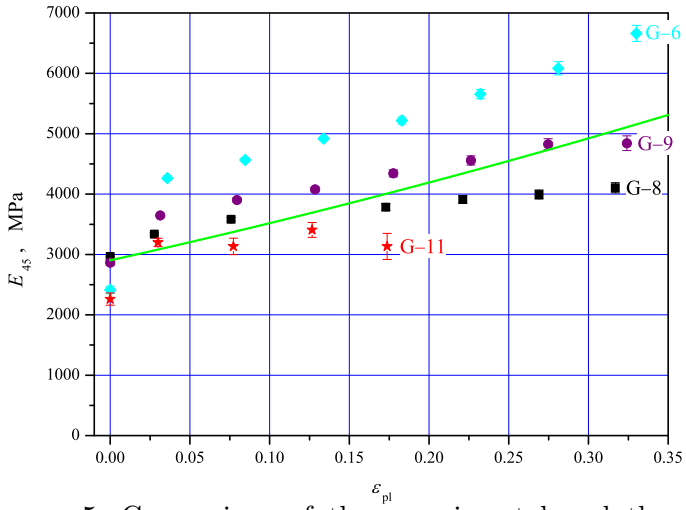

FIGURE 5. Comparison of the experimental and the predicted values for the Young modulus in the 45° direction as a function of the residual plastic strain (experimental data from [1]).

Contrary to the theory, the sample thickness increased drastically in all the samples: it reached $50 \div 90\%$ at failure, and 30% at 83 MPa engineering stress. Around the failure domain, all plies are detached from each other (so that it becomes possible to calculate their number, 20 or 40, in the sample at hand). One reason for this discrepancy is purely experimental: the large thickness values measured are the result of low pressing force used on the micrometer to measure (the detached plies are deformable). Another, theoretical, reason is related to the ideal ply interface assumption used in the present study: the displacements of the points in adjacent plies were assumed equal at all times, though it is not necessarily true up to failure.

Material failure in 45° tension experiments can be provoked by a number of different effects. Except a direct effect of the shear stress τ (or shear strain γ) exceeding some limiting value, the increase of the lateral stress (Figure 6), that is positive in all "criss" plies, while negative in all "cross" plies, can also cause failure. In the bulk of the material, since "criss" and "cross" plies always alternate, these stresses vanish in average. However, at the edges (the long side walls of the samples, in particular) these stresses should vanish, and near the edges a more complex stress field is generated, including some shear stresses at the ply interfaces. This latter stresses, similar to the case of through-thickness compression (the so-called "shear lag" effect, [3]), contribute to the samples failure. Increase of the sample's thickness, decreasing the bonds between plies, is also an effect related to failure.

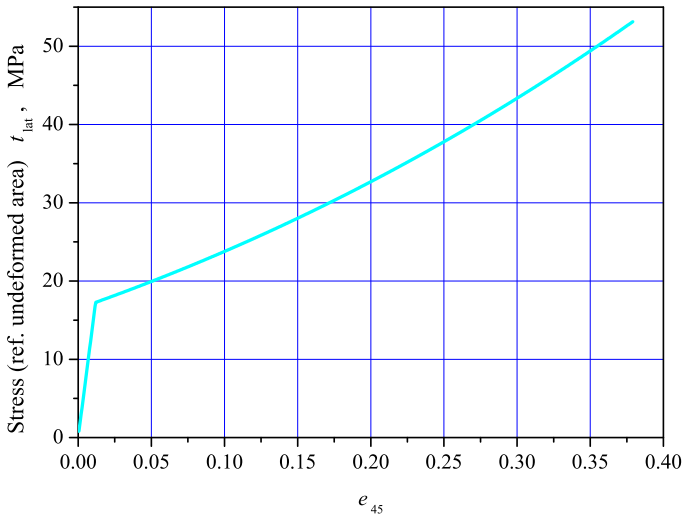

FIGURE 6. The predicted lateral engineering/first Piola–Kirchhoff stress, that appears in each ply but vanishes on average (tension in the ply plane perpendicular to the external loading direction).

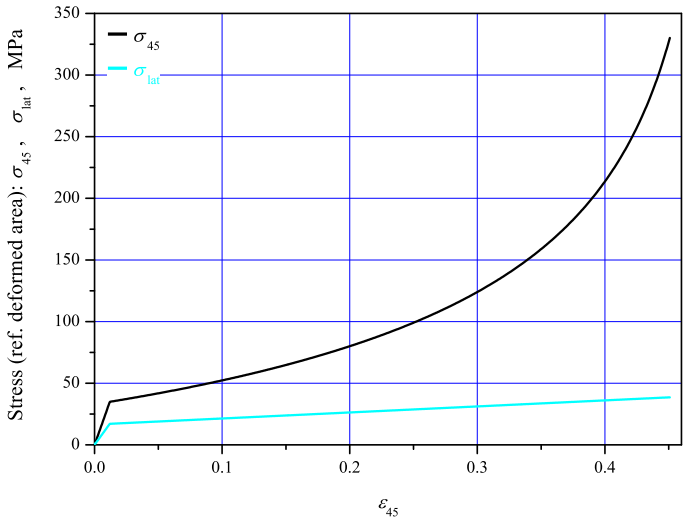

FIGURE 7. The predicted stress-strain curve in 45° tension and the lateral stress-strain curve in terms of the true (Cauchy) stress, i.e., stress calculated with reference to the deformed body area.

Let us note that the true stress on the sample (Figure 7), according to the theory predictions, reaches values around 300 MPa at failure. It is still smaller than in 0° or 90° tension but comparable.

3. Conclusion

A theoretical model of an anisotropic material, Tensylon®, under large strains is proposed. This model is capable to describe the material's response in in-plane tension at different angles to the fibrils. At 0° and at 90°, i.e. along the fibrils in either "criss" or "cross" plies, it quantitatively predicts the experimentally observed elastic behaviour until failure. At 45° to the fibrils, it quantitatively describes the experimental data in the elastic and plastic domains. The description remains accurate up to strains of 35%, that corresponds to $30 \div 40\%$ of deformation gradient components. The infinitesimal strains model would give at least 25% of error under such circumstances.

Large strain effects were considered independently of the viscoelastic effects in Tensylon® (described in [2]). Large strain viscoelastic modelling is a perspective study for Tensylon® and similar polymeric materials.

References

[1] L. Alil, M. Arrigoni, S. Badea, C. Barbu, M. Istrate, and P. Mostovykh, *On the constitutive law for the mechanical quasi-static response of criss-cross composites (on the example of UHMWPE)*, Human Factors and Mechanical Engineering for Defense and Safety **1**(1) (2017), Article 4, 12 pages.

[2] L. C. Alil, M. Arrigoni, S. M. Badea, C. Barbu, G. Bles, and P. S. Moskovykh, *Experimental study of viscoelastic properties of ultra-high molecular weight polyethylene composites (Tensylon®)*, submitted to Mechanica (2018).

[3] J. P. Attwood, S. N. Khaderi, K. Karthikeyan, N. A. Fleck,M. R. O'Masta, H. N. G. Wadley, and V. S. Deshpande, *The out-of-plane compressive response of Dyneema® composites*, Journal of the Mechanics and Physics of Solids **70** (2014), 200–226.

[4] DuPont: DuPont^{TM} Tensylon^{TM} HSBD 30A BIDIRECTIONAL LAMINATE (2013). URL http://www.dupont.com/content/dam/dupont/products-and-services/personal-protective-equipment/vehicle-armor/documents/DPP_Tensilon30A_datasheet_K25929_2.pdf

[5] DuPont protection solutions expands research on Tensylon® armor solutions. http://www.dupont.com/products-and-services/fabrics-fibers-nonwovens/fibers/press-releases/dupont-expands-research-tensylon-armor-solutions.html. Accessed: 2018-07-11

[6] P. J. Hine, I. M. Ward, N. D. Jordan, R. H. Olley, and D. C. Bassett, *A comparison of the hot-compaction behavior of oriented, high-modulus, polyethylene fibers and tapes*, Journal of Macromolecular Science, Part B: Physics **40**(5) (2001), 959–989.

[7] V. V. Novozhilov, *Foundations of the Nonlinear Theory of Elasticity*, Graylock, Rochester, 1953.

[8] V. V. Novozhilov, *Theory of Elasticity*, Elsevier, 1961.

[9] L. A. Taber, *Nonlinear Theory of Elasticity. Applications in Biomechanics*, World Scientific Publishing, Singapore, 2004.

Department of Hydraulics and Strength, Institute of Civil Engineering, Peter the Great St.Petersburg Polytechnic University, Polytechnicheskaya Str. 29, St.-Petersburg, Russia

E-mail address: mostovykh_ps@spbstu.ru; mostovykh@gmail.com